ChemPubSoc Europe

DOI: 10.1002/open.201500076

Open Access ChemistryOPEN Communications

# Morphological Transformation Reactions of Photocatalytic Metalloporphyrin-Containing Coordination Polymer Particles from Seed Structures

Yu Sun and Bongyoung Yoo*[a]

Coordination polymer particles have attracted a great deal of attention due to their characteristic properties and diverse applications in the fields of gas storage, catalysis, optics, sensing, electronics, photochemistry, and biology. Herein, we investigated shape transformation reactions of zinc 5, 10, 15, 20-tetra(4-pyridyl)-21*H*, 23*H*-porphine (ZnTPyP)-containing coordination polymer particles (ZnTPyP–CPPs) from seed structures by delicately controlling the Gibbs energy of the self-assembly system. We obtained a morphological transformation from 1D short nanorods to 1D long nanorods and 3D nano-octahedral structures, and from 3D nano-octahedral structures to 1D nanorod structures. We illustrated a new method to design and synthesize metalloporphyrin-containing CPPs in a controllable manner. Furthermore, photocatalytic properties of ZnTPyP–CPPs were tested, showing good catalytic abilities towards the photodegradation of methylene blue (MB) under visible light illumination.

Coordination polymer particles (CPPs) have attracted a great deal of attention due to their characteristic properties and diverse applications in the fields of gas storage, catalysis, optics, sensing, electronics, photochemistry, and biology.[1] In addition, CPPs usually exhibit outstanding properties compared with metal–organic frameworks (MOFs) and classic metal oxides.[2] Therefore, it is of great significance to explore the controlled synthesis of CPPs at the nano/micrometer scale.

Bottom-up and top-down strategies are two approaches to manufacture products, which were first applied to the field of nanotechnology in 1989. The top-down strategy, which includes lithography and inkjet printing of micropatterning, often uses external tools to shape materials into desired morphologies or orders.[3] However, it is quite difficult to apply this method for fragile organic materials especially for single crystals of small molecules. In contrast, the bottom-up strategy utilizes the physical or chemical properties of single molecules to synthesize various structures through self-assembly or self-organization processes.[3(a),3(d),4]

Metalloporphyrins, which are some of the most promising building blocks in the construction of diverse CPPs, have been widely utilized, and their self-assembly aggregation process can be promoted by various noncovalent interactions, including π–π, van der Waals, intermolecular electrostatic, hydrogen bonding, hydrophilic–hydrophobic, and metal–ligand coordination interactions.[5–9] As shown in Scheme 1A, various metalloporphyrin-containing CPPs with different morphological structures have been fabricated independently through self-assembly or self-organization processes.[7–9] Reversible transformation between four-petal flower structures and octahedral structures was achieved in our previous work by controlling the metalloporphyrin concentration in the reaction solvent.[10] This phenomenon suggests that different structures are possibly related to each other, and one structure can be transferred to another depending on the synthesis conditions. It was documented that the nucleation and growth of nano/microcrystals in solution are related to the Gibbs free energy, which is governed by the atomic chemical potential and surface tension of the crystals.[11] Therefore, the shape conversion could be driven

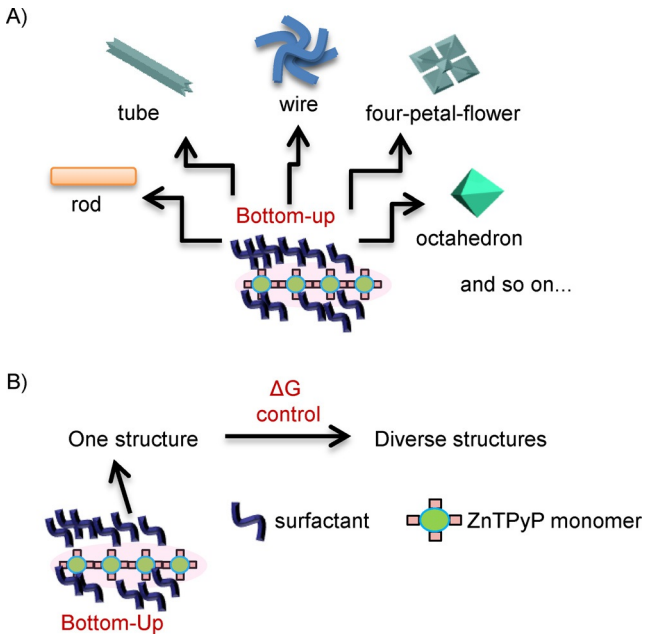


**Scheme 1.** Illustration of the traditional bottom-up method (A) and our method to synthesize ZnTPyP CPPs (B).

[a] *Dr. Y. Sun, Prof. Dr. B. Yoo*
*Department of Materials Engineering, Hanyang Univesity*
*Ansan, Gyeonggi-do 426-791 (Republic of Korea)*
*E-mail: bbyoo@hanyang.ac.kr*

Supporting information for this article is available on the WWW under http://dx.doi.org/10.1002/open.201500076.

by reducing or changing the Gibbs free energy of the investigated system, in which the atomic chemical potential could be externally influenced by pressure, temperature, reactant concentration, the solvent used in the self-assembly system, the crystal surface tension influenced by the surfactant, pH, and so on.

In this work, as shown in Scheme 1 B, we first synthesized one specific morphological structure of metalloporphyrin-containing CPPs based on zinc 5, 10, 15, 20-tetra(4-pyridyl)-21*H*, 23*H*-porphine (ZnTPyP–CPPs) through the traditional bottom-up strategy. Then, we fabricated other nanoscale structures from this "seed structure" by changing the Gibbs free energy of the self-assembled system.

As mentioned above, the Gibbs energy is the essential factor for shape conversion. Therefore, we should experimentally investigate external factors including temperature, pressure, and ZnTPyP concentration, which could impact the equilibrium between the ZnTPyP monomers and ZnTPyP aggregated particles and sequentially encourage ZnTPyP particles to re-aggregate in the reconstructed micelles,. First, a series of experiments was carried out by injecting a ZnTPyP stock solution (250 μL of 0.01 M) into the basic stock solution A (5 mL) which was prepared by dissolving Pluronic F-127 (4 g) and NaOH (0.0125 g) in an aqueous solution (200 mL), under vigorous stirring for 1 h at different temperatures (Figure S1 in the Supporting Information). It was found that not only nanorod structures, but also nanotube and octahedral structures can be synthesized at different temperatures, which confirmed that the micelle formation changes depending on the temperature. Then, the ZnTPyP self-assembly process was investigated by injecting a ZnTPyP stock solution (250 μL of 0.01 M) into basic stock solution A (5 mL) at room temperature and a low atmospheric pressure (~0.7 Pa). However, uniform structures were not fabricated (Figure S2 in the Supporting Information). Finally, the effect of the ZnTPyP concentration on the shape evolution of ZnTPyP–CPPs was investigated by injecting a ZnTPyP stock solution (150, 350, and 450 μL of 0.01 M) into basic stock solution A (5 mL) at room temperature. It was observed that rod-like structures were fabricated at a low ZnTPyP concentration and oval-like structures with terraces were preferentially formed at a high ZnTPyP concentration (Figure S3 in the Supporting Information). As a result, we confirmed that the morphological structures of ZnTPyP–CPPs are strongly influenced by the Gibbs energy of the investigated system and there is the possibility to convert one specific structure to other structures by tuning the Gibbs energy.

In the nanoscale morphological transformation experiments, seed structures were first synthesized. Typically, a ZnTPyP stock solution (250 μL of 0.01 M) was added into the basic stock solution A (5 mL) under vigorous stirring for 1 h at room temperature. This solution was the seed solution, abbreviated as Seed-1. The same experiment was also carried out at 100 °C and the obtained seed-structure solution was abbreviated as Seed-2. The external morphology and size of the ZnTPyP–CPPs synthesized in the Seed-1 and Seed-2 solutions were characterized by scanning electron microscopy (SEM) and transmission electron microscopy (TEM). As shown in Figure 1 A, large-scale and uniform formation of one-dimensional (1 D) hexagonal nanorods occurred in the Seed-1 solution. The TEM image (Figure 1 B) shows a solid structure of nanorods with an average diameter of ~80 nm and an average length of ~170 nm. Compared to the 1 D nanorod structures, three-dimensional (3 D) nano-octahedral structures were fabricated in the Seed-2 solution (Figure 1 C). The TEM image (Figure 1 D) clearly reveals that the obtained nano-octahedral structures have a typical 3 D architecture with an average side length of ~100 nm. The internal microstructures of the ZnTPyP–CPPs synthesized in both the Seed-1 and Seed-2 solutions were investigated by X-ray diffraction (XRD) measurements. As can be seen in Figure S4 in the Supporting Information, the ZnTPyP CPPs with different morphologies exhibited similar XRD patterns, which matched the simulated pattern on the basis of a former study of the crystal structures of ZnTPyP compounds.[12] An interlattice distance of 1.632 nm was derived from diffraction peaks at $2\theta = 5.24^\circ$ and $10.54^\circ$ in the XRD patterns of the nanorod structures synthesized in the Seed-1 solution and the nano-octahedral structures in the Seed-2 solutions. The average width of nanorod structures can be roughly calculated as ~70 nm from the diffraction peak at $2\theta = 10.54^\circ$ according to the Scherrer equation, which is in accordance to the width of nanorod structures measured from the SEM and TEM images. In addition, it is clearly seen that the characteristic peak attributed to (220) is remarkably intense in the nanorod structures, compared to that of the nano-octahedral structures, which is probably due to the preferential growth along the crystallographic *c* axis in nanorod structures.[13]

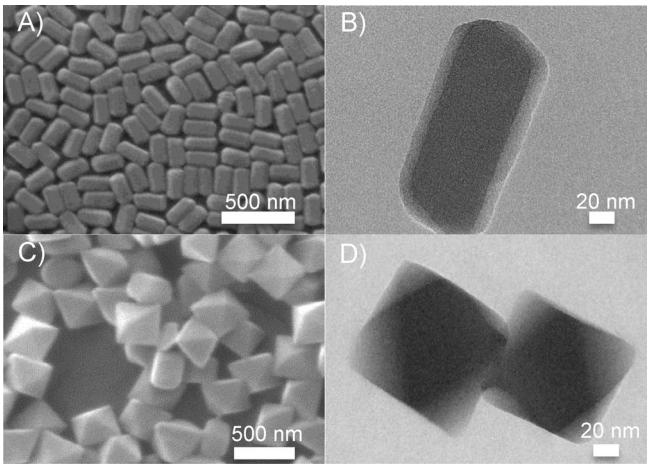


**Figure 1.** SEM images of the nanorod structures produced in the Seed-1 solution (A) and nano-octahedral structures fabricated in the Seed-2 solution (C); TEM images of the nanorod structures produced in the Seed-1 solution (B) and nano-octahedral structures fabricated in the Seed-2 solution (D).

When the Seed-1 solution was kept at room temperature under continuously vigorous stirring for 15 h, no rod growth was observed (Figure 2, route 1). However, the average length of the nanorods in the Seed-1 solution grew to ~395 nm when the reaction temperature was increased to 100 °C under vigorous stirring for 15 h. (Figure 2, route 2). The rod growth was facilitated by only adjusting the reaction temperature. Figure S5 in the Supporting Information shows the SEM images

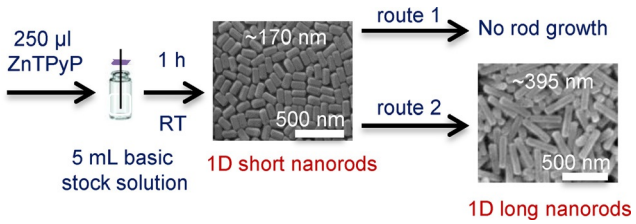


**Figure 2.** Illustration of the shape transformation from short nanorod structures to long nanorod structures.

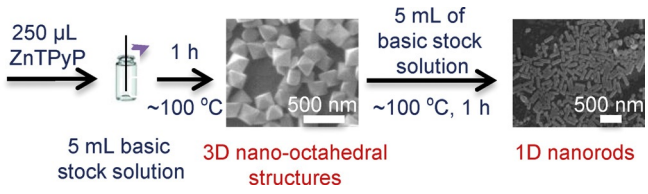


**Figure 4.** Illustration of the shape transformation from nano-octahedral structures to nanorod structures.

obtained at different reaction times. We observed that the nanorod structures were destroyed within several hours. However, the regrowth was established when the reaction time was increased to 15 h.

The shape conversion within the same dimension was relatively easier as the growth direction was not changed. It is quite difficult to convert 1D short nanorods to 3D nano-octahedral structures. The temperature-dependence experiments revealed that nano-octahedral structures were synthesized at 100 °C, which indicates that the micelle formation of Pluronic F-127 at 100 °C is suitable for the fabrication of octahedral structures. On the other hand, the nanorods in the Seed-1 solution did not change into octahedral structures when it was directly transferred into the 100 °C oil bath without any other treatment, which indicates that shape conversion from the nanorod to an octahedral structure cannot be achieved only by temperature adjustment (Figure 3, route 1). In our opinion,

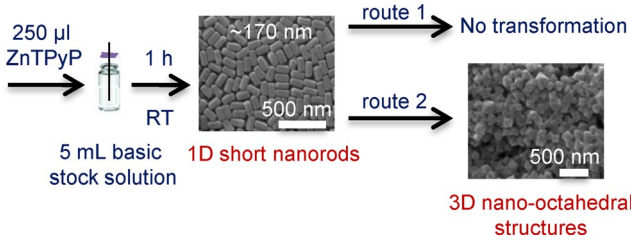


**Figure 3.** Illustration of the shape transformation from short nanorod structures to nano-octahedral structures.

there are usually two ways to convert one structure to another: the first one is to break the original structure to form a new one under new conditions, and the other method is continuous growth on the original structure. Therefore, the conversion from the nanorod structures to octahedral structures could belong to the latter case, in which an additional amount of the ZnTPyP stock solution should be supplied.

We carried out a series of experiments by first transferring the Seed-1 solution into the 100 °C oil bath. Then, different amounts of the ZnTPyP stock solution were injected into the Seed-1 solution under vigorous stirring for 1 h. It was found that nanorods were transformed into nano-octahedral structures when 550 µL of the ZnTPyP stock solution was added after being transferred into the oil bath (Figure 3, Route 2). When the amount of the ZnTPyP stock solution was less than 550 µL, octahedral structures with terraces were fabricated, which clearly illustrates the ZnTPyP growth on the nanorod structure. On the other hand, as shown in Figure 4, nano-octahedral structures synthesized in the Seed-2 solution were successfully transformed into nanorods when 5 mL of the basic stock solution A was injected into the Seed-2 solution at 100 °C under vigorous stirring for 6 h. A trace amount of disordered structures was also synthesized as side products.

The porphyrin aggregation and its aggregation type can be detected through the spectrum changes of the degenerated Soret band in its characteristic UV/Vis spectrum.[10,13] Figure S6 in the Supporting Information compares the electronic absorption spectra of short nanorods synthesized in the Seed-1 solution (Figure S6B), long nanorods transformed from short nanorods (Figure S6C), nano-octahedral structures transformed from short nanorods (Figure S6D), nano-octahedral structures synthesized in the Seed-2 solution (Figure S6E), and nanorods transformed from nano-octahedral structures (Figure S6F). As a reference, the electronic structure of the ZnTPyP monomer (Figure S6A) which was prepared by dissolving commercial ZnTPyP in an HCl solution was determined. We confirmed that both ZnTPyP–CPPs synthesized in the seed structure solutions and those synthesized by morphological transformation reactions exhibit J-type aggregation with an edge-to-edge molecular arrangement by observing the split and blue-shifted Soret bands, with respect to the ZnTPyP monomer.[10]

The fluorescent properties were measured by fluorescent spectroscopy and fluorescent microscopy (FM). As shown in Figure S7 in the Supporting Information, upon excitation at the ZnTPyP Soret band wavelength (around 425 nm), the photoluminescence emission spectrum of the ZnTPyP monomer showed one wide emission band, and those of the ZnTPyP–CPPs synthesized in the seed solutions and by the morphological transformation reactions showed two intense emission bands in the wavelength range from 600 to 700 nm, which correspond to J-type aggregation and are in good agreement with the UV/Vis experimental results.[13] The FM images further confirmed that all ZnTPyP–CPPs are fluorescent in the red region of the spectrum (Figure S7).

As a member of the porphyrin family, ZnTPyP shares a similar molecular structure to its photoactive counterparts such as chlorophyll and heme. Therefore, we investigated the photocatalytic ability of ZnTPyP–CPPs for methylene blue (MB) photodegradation under visible light irradiation. Figure S8A in the Supporting Information shows the photocatalytic degradation of MB dye as a function of time by measuring the UV/Vis absorption spectra. For a better comparison, MB decomposition without catalysts and with P25 $TiO_2$ catalysts was also investi-

gated. The absorption spectra without catalyst (Figure S8 A) and with P25 $TiO_2$ catalysts (Figure S8 B) did not change significantly as a function of time, indicating that P25 $TiO_2$ does not act as a photocatalyst for the MB decomposition under visible light illumination because of its poor visible-light absorption capability.[14] However, irradiating the reaction slurry with visible light results in a gradual and steady decrease of the absorption peak formed at $\lambda_{max} = 664$ nm in the presence of ZnTPyP–CPPs. The percentage of dye degradation, η was calculated as follows

$$\eta = \frac{(A_0 - A)}{A} \times 100\% \quad (1)$$

where $A_0$ is the initial absorbance of the dye and $A$ is the time-dependent absorbance. We plotted the percentage of dye residue ($1-\eta$) after 5 h of illumination. As shown in Figure 5, ~75%, 68%, and 56% of MB dye was decomposed by ZnTPyP–CPP long nanorods synthesized from Seed-1 solution, ZnTPyP–CPPs with nano-octahedral structures synthesized from Seed-1 solution, and ZnTPyP–CPP nanorods synthesized from Seed-2 solution, respectively, compared to ~12% MB degradation without catalysts or in the presence of P25 TiO2.

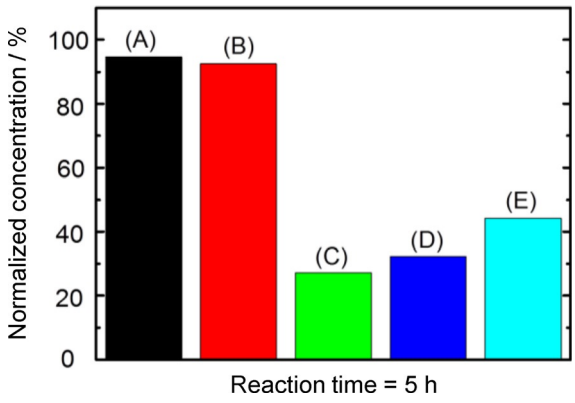


**Figure 5.** Comparison of photocatalytic decomposition of methylene blue without catalysts (A), with P25 $TiO_2$ (B), and with ZnTPyP–CPPs with long nanorod structures synthesized from Seed-1 (C), nano-octahedral structures synthesized from Seed-1 (D), and nanorod structures synthesized from Seed-2 (E) as catalysts under visible light illumination for 5 h.

It has been reported that the formation of J-type aggregation favors the electron transfer in photocatalytic reactions.[15] It is clearly seen from Figure S6 in the Supporting Information that ZnTPyP–CPPs with long nanorod structures synthesized from Seed-1 were aggregated in a more complete way. Whereas, the J-type aggregation in ZnTPyP–CPPs with nano-octahedral structures synthesized from Seed-1 solution and ZnTPyP–CPPs with nanorod structures synthesized from Seed-2 solution were less complete as the Soret band in these two structures was not well separated. We hypothesize that photocatalytic differences found in our work may be caused by the extent of J-type aggregation. More experiments are under way to study the size- and shape-dependent photocatalytic properties of ZnTPyP–CPPs.

In conclusion, fluorescent 1D short nanorod structures and 3D nano- octahedral structures of ZnTPyP-containing CPPs were synthesized through a traditional bottom-up strategy assisted by Pluronic F-127 as a surfactant in an aqueous solution and were utilized as seed structures for further morphological transformation reactions. For the first time, morphological transformations from 1D short nanorods to 1D long nanorods and 3D nano-octahedral structures and from 3D nano-octahedral structures to 1D nanorods were successfully achieved by delicately controlling the Gibbs energy of the system. This demonstrates a new strategy to synthesize fluorescent metalloporphyrin-containing CPPs in a reasonable and controllable manner. The electronic adsorption spectra obtained by UV/Vis spectroscopy revealed that J-type aggregation existed in both ZnTPyP–CPPs synthesized in the seed structures and those synthesized by the shape-transformation reactions. All ZnTPyP–CPPs are fluorescent in the red region of the spectrum, which was confirmed by fluorescent spectroscopy and fluorescent microscopy. In addition, all ZnTPyP–CPPs synthesized from morphological transformation reactions exhibit good photocatalytic abilities towards methylene blue dye decomposition under visible light illumination.

## Acknowledgements

*This work was supported by the Strategic Core Materials Technology Development Program (No. 10043799), the New & Renewable Energy Technology Development Program of the Korea Institute of Energy Technology Evaluation and Planning (KETEP) (No. 20123010010160), the Ministry of Trade, Industry & Energy (MOTIE), Korea (10048778), and the Korea Semiconductor Research Consortium (KSRC) support program for the development of the future semiconductor devices.*

**Keywords:** coordination polymer particles · metalloporphyrin · morphological transformation · photocatalytic degradation

[1] a) W. Cho, H. J. Lee, M. Oh, *J. Am. Chem. Soc.* **2008**, *130*, 16943 – 16946; b) M. Oh, C. A. Mirkin, *Angew. Chem. Int. Ed.* **2006**, *45*, 5492 – 5494; *Angew. Chem.* **2006**, *118*, 5618 – 5620; c) M. Oh, C. A. Mirkin, *Nature* **2005**, *438*, 651 – 654; d) P. Horcajada, C. Serre, M. Vallet-Regi, M. Sebban, F. Taulelle, G. Ferey, *Angew. Chem. Int. Ed.* **2006**, *45*, 5974 – 5978; *Angew. Chem.* **2006**, *118*, 6120 – 6124; e) L. H. Wee, S. R. Bajpe, N. Janssens, I. Hermans, K. Houthoofd, C. E. A. Kirschhock, J. A. Martens, *Chem. Commun.* **2010**, *46*, 8186 – 8188; f) Y.-D. Chiang, M. Hu, Y. Kamachi, S. Ishihara, K. Takai, Y. Tsujimoto, K. Ariga, K. C.-W. Wu, Y. Yamauchi, *Eur. J. Inorg. Chem.* **2013**, 18, 3141 – 3145; g) M. Hu, S. Ishihara, Y. Yamauchi, *Angew. Chem. Int. Ed.* **2013**, *52*, 1235 – 1239; *Angew. Chem.* **2013**, *125*, 1273 – 1277.

[2] a) A. Facchetti, *Mater. Today* **2007**, *10*, 28 – 37; b) A. L. Briseno, S. C. B. Mannsfeld, S. A. Jenekhe, Z. Bao, Y. Xia, *Mater. Today* **2008**, *11*, 38 – 47; c) A. C. Grimsdale, K. Mullen, *Angew. Chem. Int. Ed.* **2005**, *44*, 5592 – 5629; *Angew. Chem.* **2005**, *117*, 5732 – 5772.

[3] a) A. Biswas, I. S. Bayer, A. S. Biris, T. Wang, E. Dervishi, F. Faupel, *Adv. Colloid Interface Sci.* **2012**, *170*, 2 – 27; b) J. S. Chen, T. Zhu, X. H. Yang, H. G. Yang, X. W. Lou, *J. Am. Chem. Soc.* **2010**, *132*, 13162 – 13164; c) M. Pumera, *Chem. Soc. Rev.* **2010**, *39*, 4146 – 4157; d) L. J. Zhang, T. J. Webster, *Nano Today* **2009**, *4*, 66 – 80.

[4] a) M. Shimomura, T. Sawadaishi, *Curr. Opin. Colloid Interface Sci.* **2001**, *6*, 11 – 16; b) S. B. Yang, Y. J. Gong, Z. Liu, L. Zhan, D. P. Hashim, L. L. Ma, R. Vajtai, P. M. Ajayan, *Nano Lett.* **2013**, *13*, 1596 – 1601; c) W. Lu, C. M.

 

Lieber, *Nat. Mater.* **2007**, *6*, 841 – 850; d) R. Murugavel, M. G. Walawalkar, M. Dan, H. W. Roesky, C. N. R. Rao, *Acc. Chem. Res.* **2004**, *37*, 763 – 774.

[5] a) L. X. Jiang, J. W. J. de Folter, J. B. Huang, A. P. Philipse, W. L. Kegel, A. V. Petukhov, *Angew. Chem. Int. Ed.* **2013**, *52*, 3364 – 3368; *Angew. Chem.* **2013**, *125*, 3448 – 3452; b) C. H. Yu, L. Zhao, S. J. Wang, Z. P. Cui, J. Peng, J. Q. Li, M. L. Zhai, J. B. Huang, *Soft Matter* **2013**, *9*, 5959 – 5965; c) R. P. Andres, J. D. Bielefeld, J. I. Henderson, D. B. Janes, V. R. Kolagunta, C. P. Kubiak, W. J. Mahoney, R. G. Osifchin, *Science* **1996**, *273*, 1690 – 1693; d) M. Fujita, D. Oguro, M. Miyazawa, H. Oka, K. Yamaguchi, K. Ogura, *Nature* **1995**, *378*, 469 – 471; e) K. Kadish, K. M. Smith and R. Guilard, *Porphyrin Handbook*, Academic Press, New York, **1999**; f) W. M. Campbell, K. W. Jolley, P. Wagner, K. Wagner, P. J. Walsh, K. C. Gordon, L. Schmidt-Mende, M. K. Nazeerudding, Q. Wang, M. Gratzel, D. L. Officer, *J. Phys. Chem. C* **2007**, *111*, 11760 – 11762; g) C. Yao, L. Yan, L. Guan, C. Liu, P. Song, Z. Su, *Dalton Trans.* **2010**, *39*, 7645 – 7649.

[6] a) S. Thyagarajan, T. Leiding, S. P. Arsköld, A. V. Cheprakov, S. A. Vinogradov, *Inorg. Chem.* **2010**, *49*, 9909 – 9920; b) S. M. Ribeiro, A. C. Serra, A. M. d'A Rocha Gonsalves, *J. Mol. Catal. A: Chem.* **2010**, *326*, 121 – 127; c) A. Verma, S. L. Facchina, D. J. Hirsch, S. Song, L. F. Dillahery, J. R. Willians, S. H. Synder, *Mol. Med.* **1998**, *4*, 40 – 45.

[7] a) V. E. Yushmanov, T. T. Tominaga, I. E. Bobrissevitch, H. Imasato, M. Tabak, *Magn. Reson. Imaging* **1996**, *14*, 255 – 261; b) K. Komagoe, T. Katsu, *Anal. Sci.* **2006**, *22*, 255 – 258.

[8] a) F. Bai, H. M. Wu, R. E. Haddad, Z. C. Sun, S. K. Schmitt, V. R. Skocypec, H. Y. Fan, *Chem. Commun.* **2010**, *46*, 4941 – 4943; b) F. Bai, Z. C. Sun, H. M. Wu, R. E. Haddad, E. N. Coker, J. Y. Huang, M. A. Rodriguez, H. Y. Fan, *Nano Lett.* **2011**, *11*, 5196 – 5200; c) J. S. Hu, Y. G. Guo, H. P. Liang, L. J. Wan, L. Jiang, *J. Am. Chem. Soc.* **2005**, *127*, 17090 – 17095.

[9] a) Y. F. Qiu, P. L. Chen, M. H. Liu, *J. Am. Chem. Soc.* **2010**, *132*, 9644 – 9652; b) P. P. Guo, P. L. Chen, M. H. Liu, *Langmuir* **2012**, *28*, 15482 – 15490.

[10] a) Y. Sun, B. Y. Yoo, *CrystEngComm* **2014**, *16*, 8950 – 8953; b) Y. Sun, B. Y. Yoo, *N. J. Chem.* **2015**, *39*, 3366 – 3370.

[11] a) S. Kudera, L. Carbone, L. Manna, W. L. Parak, *Semiconductor Nanocrystal Quantum Dots Synthesis Assembly, Spectroscopy and Applications: Growth Mechanism, Shape and Composition Control of Semiconductor Nanocrystals*, Springer, Berlin, New York, **2008**, pp. 5 – 6; b) J. J. Ning, K. K. Men, G. J. Xiao, L. Wang, Q. Q. Bai, B. Zou, B. B. Liu, G. T. Zou, *Nanoscale* **2010**, *2*, 1699 – 1703; c) D. A. Porter, K. E. Easterling and M. Y. Sherif, *Phase Transformations in Metals and Alloys, Vol. 2*, CRC Press, Weinheim, **2008**, pp. 111 – 117.

[12] a) S. H. Im, U. Jeong, Y. Xia, *Nat. Mater.* **2005**, *4*, 671 – 675; b) H. Krupitsky, z. Stein, I. Goldberg, C. E. J. Strouse, *J. Inclusion Phenom. Mol. Recognit. Chem.* **1994**, *18*, 177 – 192; c) K. J. Lin, *Angew. Chem. Int. Ed.* **1999**, *38*, 2730 – 2732; *Angew. Chem.* **1999**, *111*, 2894 – 2897.

[13] W. Sun, H. L. Wang, D. D. Qi, L. Wang, K. Wang, J. L. Kan, W. J. Li, Y. L. Chen, J. Z. Jiang, *CrystEngComm* **2012**, *14*, 7780 – 7786.

[14] a) J. L. Vivero-Escoto, Y. D. Chiang, K. C-W. Wu, Y. Yamauchi, *Sci. Technol. Adv. Mater.* **2012**, *13*, 013003; b) H. Oveisi, S. Rahighi, X. Jiang, Y. Nemoto, A. Beitollahi, S. Wakatsuki, Y. Yamauchi, *Chem. Asian J.* **2010**, *5*, 1978 – 1983.

[15] P. Guo, P. Chen, W. Ma, M. Liu, *J. Mater. Chem.* **2012**, *22*, 20243 – 20249.

Received: March 23, 2015
Published online on May 20, 2015

 